Geomechanics and Engineering, *Vol. 30, No. 3 (2022) 281-291*
https://doi.org/10.12989/gae.2022.30.3.281

Analysis of the mechanical properties and failure modes of rock masses with nonpersistent joint networks

Yongning Wu[1a], Yang Zhao[1b], Peng Tang[1c], Wenhai Wang[1d] and Lishuai Jiang*[1,2]

[1]*State Key Laboratory of Mining Disaster Prevention and Control, Shandong University of Science and Technology, Qingdao 266590, China*
[2]*Shandong Key Laboratory of Civil Engineering Disaster Prevention and Mitigation, Shandong University of Science and Technology, Qingdao 266590, China*

(*Received April 22, 2021, Revised July 17, 2022, Accepted July 18, 2022*)

Abstract. Complex rock masses include various joint planes, bedding planes and other weak structural planes. The existence of these structural planes affects the mechanical properties, deformation rules and failure modes of jointed rock masses. To study the influence of the parameters of a nonpersistent joint network on the mechanical properties and failure modes of jointed rock masses, synthetic rock mass (SRM) technology based on discrete elements is introduced. The results show that as the size of the joints in the rock mass increases, the compressive strength and the discreteness of the rock mass first increase and then decrease. Among them, the joints that are characterized by "small but many" joints and "large and clustered" joints have the most significant impact on the strength of the rock mass. With the increase in joint density in the rock mass, the compressive strength of rock mass decreases monotonically, but the rate of decrease gradually decreases. With the increase in the joint dip angle in rock mass, the strength of the rock mass first decreases and then increases, forming a U-shaped change rule. In the analysis of the failure mode and deformation of a jointed rock mass, the type of plastic zone formed after rock mass failure is closely related to the macroscopic displacement deformation of the rock mass and the parameters of the joints, which generally shows that the location and density of the joints greatly affect the failure mode and displacement degree of the jointed rock mass. The instability mechanism of jointed surrounding rock is revealed.

Keywords: discrete fracture network; jointed rock mass; nonpersistent joint; synthetic rock mass technique

1. Introduction

Complex rock masses include various joint planes, bedding planes and other weak structural planes. The existence of these structural planes affects the mechanical properties, deformation rules and various failure modes of jointed rock masses. The mechanical properties of rock masses play an important role in the construction of large rock mass engineering projects, such as dams, foundation pits, underground chambers, and nuclear power plants foundations (Wang *et al*. 2017). Rock mass failure is the process by which these weak structural planes develop and connect to form macroscopic fractures and ultimately fail and become unstable. Joints, as a common structural plane, are an important factor affecting the mechanical properties of rock. The density, angle, size and nonuniformity of the joints in the rock mass lead to nonlinear changes and anisotropy in its failure process. The spatial distribution of joints and the joint combination rule directly control the stability of rock mass engineering and the possible failure modes. Therefore, this distribution provides a basis for engineering design, deformation calculation, and stability evaluation (Mughieda 1997).

The long, uniform, and persistent joints in a natural rock mass account for only a small number of the total number of joints; most joints are short, nonpersistent and nonuniformly distributed. At the same time, engineering activities such as engineering construction, roadway excavation and engineering site selection have been designed to avoid large-scale persistent joints as much as possible, and nonpersistent jointed rock masses have become more commonly encountered in rock mass engineering (Wang *et al*. 2017). Therefore, studying the influences of the angle, density, spatial distribution and size of nonpersistent joints on the mechanical properties and failure modes of rock masses has great scientific significance and application value. In the fields of civil engineering, mining, transportation and other rock mass engineering, such studies have far-reaching significance. At present, research on the deformation characteristics and failure modes of jointed rock masses is mainly divided into laboratory experiments and numerical experiments. Although laboratory experiments such as empirical analogy and theoretical analysis under simplified conditions have

*Corresponding author, Professor
E-mail: lsjiang@sdust.edu.cn
[a]M.Sc. Student
E-mail: yongningwu2021@163.com
[b]M.Sc. Student
E-mail: mrzhao_y@163.com
[c]M.Sc. Student
E-mail: tpsdustenactus@163.com
[d]M.Sc. Student
E-mail: wenhaiwang2020@163.com

ISSN: 2005-307X (Print), 2092-6219 (Online)

solved many problems, due to the complexity and variability of the natural and engineering environment of a rock mass, a variety of factors, such as the size of the rock mass, the lithology of the rock mass, and the distribution of joints, greatly affect its strength and failure modes. In particular, it is difficult to accurately calculate, simulate and predict the results in a complex geographic environment under actual engineering conditions, so this paper mainly uses numerical simulation to study the influence of nonpersistent joints on the mechanical properties and failure modes of rock masses (Yin *et al*. 2012). Meng *et al*. (2012) studied the distribution law of plastic zone of roadway with different cross-section shape by numerical simulation method, and optimized the roadway cross-section shape. Zeng *et al*. (2019) adopted 3DEC discrete element numerical simulation software to analyze the plastic zone of roadway surrounding rock in a mining area, and combined with the field measured data, put forward the support scheme of "bolt+anchor cable+steel belt".

With the development of computer technology, numerical simulation methods based on discontinuous media have become widely used. In the numerical simulation calculations, a single joint or multiple joints are prefabricated in the rock mass to be tested under uniaxial loading, and the influences of mesoscopic parameters such as the angle, density and quantity of the joints on the mechanical properties of the rock mass are studied, so a wide range of engineering problems can be solved. Zhu *et al*. (2003) simulated the influence of angle and strike on rock mass breakage in the loading process of a rock mass with a single joint with RFPA2D and analyzed the change in rock mass strength and breakage characteristics. Zhao *et al*. (2019) used the three-point modeling method in 3DEC to build rock mass models containing a single joint and multiple joints and conducted tensile experiments on these models to analyze the relationship between the change in parameters such as the elastic modulus and rock mass strength. Zhao *et al*. (2020), Huang *et al*. (2016), Huang and Yang (2015) carried out uniaxial compression experiments on specimens containing two groups of cross-fractured rock masses by PFC3D particle flow software and analyzed the strength and failure mode of jointed rock masses by adjusting the joint angle, confining pressure and position and other parameters. In recent years, these studies have focused on mainly single-joint or multiple-joint rock mass models. The rock mass strength, elastic modulus, and failure mode are effectively analyzed by changing the angle, size, density and other mesoscale parameters. Although this simplified processing approach speeds up the calculation, it also ignores the complexity of the jointed rock mass, and some errors and limitations arise in the analysis of the results. At the same time, the number and distribution of joints in actual engineering are random and uncertain. At present, considering the actual distribution of joints collected at engineering sites, the numerical simulation SRM rock mass synthesis technology and the discrete fracture network (DFN) technology proposed by Huang and Yang (2015) have attracted the attention of scholars domestically and abroad. Ivars *et al*. (2011) established a two-dimensional fracture network model with RFPA2D and studied the mechanical properties and deformation characteristics of rock masses under uniaxial compression. Shungui *et al*. (2008) used Monte Carlo stochastic simulation technology to generate a two-dimensional seepage model of a fracture network and studied the flow characteristics of water in a fracture network under different boundary conditions. Wang *et al*. (2019) established a rock mass model of a fracture network with 3DEC to study the effect of equivalent mechanical parameters of a jointed rock mass on its structural behavior. In this paper, the discrete fracture network (DFN) technique is used to simulate the random distribution of fractures observed in actual engineering, and the effects of fracture parameters on the mechanical properties and failure modes of rock masses are analyzed by mathematical statistical methods. With the in-depth study of the impact of joint mesoscale parameters on the mechanical properties and deformation of rock masses, domestic and foreign scholars have conducted extensively and systematically researched and discussed joint angle, joint density and other parameters. By analyzing the evolution characteristics of different joints, Olofsson and Fredriksson (2005) studied the effect of joint angle on the damage degree of a rock mass and revealed that with increasing joint angle, the rock mass strength presents an inverted "U" distribution. Li *et al*. (2006) analyzed the influence of joint geometric characteristics on the overall deformation and strength of rock masses by studying the mechanical properties of jointed rock masses. However, there are few studies on rock masses with three-dimensional nonpersistent fracture networks.

This numerical simulation work is based on SRM rock mass synthesis technology. 3DEC discrete element simulation software is combined with virtual joint technology. Then, according to the field statistical results, the joint distribution is simulated by a power law function, and a DFN-DEM rock mass model is constructed. This experimental work simulates the mechanical properties and anisotropy of fractured rock masses and analyzes the influence of the joint angle, density, and size on the compressive strength, deformation characteristics and failure modes of rock masses. The above research methods can be directly applied to establish discrete element numerical models of complex nonpersistent fractured rock masses and study the mechanical behavior of jointed rock masses.

2. 1 Model establishment

Synthetic rock mass (SRM) technology was proposed by Ivars *et al*. (2011). In this method, a discrete fracture network (DFN) and a block discrete element model (DEM) are separately constructed and then the DFN model is used to cut the DEM model to obtain a new DFN-DEM discrete element numerical calculation model. The DFN-DEM model is loaded and unloaded, and the various mechanical behaviors and related results of the rock mass are analyzed. At present, the numerical software mainly used for synthetic rock mass technology includes PFC3D based on particle flow and 3DEC based on block discrete elements.

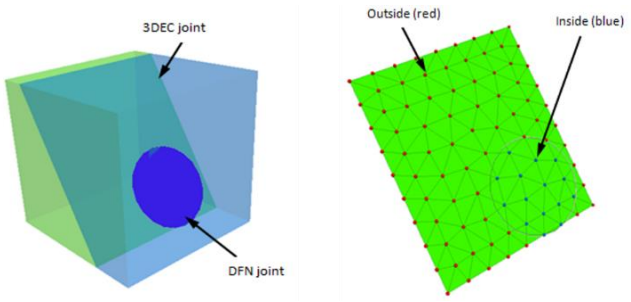

Fig. 1 Mesh grid of topographic model

In this study, virtual joint technology in 3DEC was used to study the mechanical properties and failure mode of jointed rock masses through the built-in DFN module (Esmaieli *et al*. 2010). The DFN model is derived from the results of mathematical statistics in the rock mass, the basic information of the joints in the rock mass is obtained according to field surveys, and the corresponding parameter characteristics are obtained by combining the probability distribution form from mathematical statistics (Deng *et al*. 2020). In principle, the discrete element method can consider only the problem of throughgoing joints and cannot effectively calculate a solution for nonpersistent joints. Therefore, the DFN model in 3DEC is improved and replaced by virtual joints (Harthong *et al*. 2012, Bo 2010, Cheng-Fu and Wang 2015). In a DFN, it is assumed that the diameter of each disc is finite. Since the 3DEC block cannot be partially cut, it is divided according to the contact unit of the disc, and mechanical parameters of different properties are assigned to the inside and outside of the disc so that a disc fracture surface is formed. According to a large number of calculations and verifications, good results can be obtained when the external parameters of the disc are more than 10 times greater than the internal parameters of the disc (Huang *et al*. 2014), so the properties of the rock mass after the parameters are given are the same as when no joints are added (see equations (1) and (2)). This numerical simulation adopts the method provided by the 3DEC Manual (Inc 2013), as shown in Fig. 1

$$G/Kjs = 0.08 - 0.012 \quad (1)$$

$$Kjn/Kjs = 2 - 3 \quad (2)$$

where *G*, *Kjs*, and *Kjn* are the whole rock shear modulus, the shear stiffness of the virtual joint, and the normal stiffness of the virtual joint respectively.

Taking into account the computational efficiency of the model and computational time required, *G/Kjs*=0.01. The model and joint parameters obtained by consulting data and laboratory experiments are shown in Table 1.

In this paper, the DEM model has a height of 10.0 cm and diameter of 5.0 cm, and the DFN is established with a height of 10.0 cm and width and length of 1.8 cm. In the numerical experiment of jointed rock mass, the joint information mainly includes occurrence, spacing, ductility and fillers, among which the parameter information that can best represent the spatial characteristics of joints is dip angle, diameter and density. At the same time, the same fracture network characterization parameters will generate

Table 1 Rock mass properties (Shu *et al*. 2019)

Lithology	Density (kg/m^3)	Bulk Modulus *K* (GPa)	Shear modulus *G* (GPa)	Cohesion C (MPa)	Internal friction angle φ (°)	Tensile strength (MPa)
Sandstone	2630	26.49	19.05	3.75	25.9	2.25

Table 2 Joint properties (Shu *et al*. 2019)

Lithology	Cohesion *C* (MPa)	Bulk Modulus *K* (GPa)	Shear modulus *G* (GPa)	Joint friction angle φ (°)	Tensile strength (MPa)
Sandstone	3.67	26.49	19.05	25.9	1.88

countless numbers in the numerical simulation process. Although these fracture networks have the same meaning in mathematics and statistics, the rock mass models formed by different fracture networks must have random and different rock mass mechanical properties. Therefore, the results of any fracture network-rock mass model cannot be regarded as a statistically deterministic result. The mechanical properties of the fracture network-rock mass model are set as the average values after several simulations. Therefore, in this paper, the fracture network is set by different. In order to better reflect the randomness and uncertainty of fractures, the random factors of fracture networks are set for 10 times in this paper, and different fracture structures under the same parameters are obtained. by taking the mean and standard deviation of uniaxial compressive strength of jointed rock mass with different spatial distribution under the same parameters, the influence of randomness is weakened and the reliability of experimental results is increased. In the uniaxial compression experiment in this paper, the loading speed of the numerical experiment is mainly based on the physical experiment. Combined with the previous literature and experimental results, the loading speed is consistent with the physical experimental speed, which is 3×10^{-5} cm/per cycle step, and a uniaxial compression test is performed to calculate the uniaxial compressive strength of the rock mass. The specific process is as follows:

3. The influence of the spatial distribution of joints on the mechanical properties of rock masses

3.1 The influence of the spatial distribution of joints on the compressive strength of the rock mass

DFN model is a set of statistical distributions that define the geometric characteristics of joint fracture networks: fracture size, direction and location, density and random seed number. To study the influence of the spatial distribution of the joints on the mechanical properties of the rock mass, the diameter *D* range of the joints is increased from 0.45-0.55 cm to 3.45-3.55 cm. The power law distribution and control variable method are used. The joint positions and angles are randomly distributed. There is a correlation between the number of joints and joint size per unit volume, as shown in Eqs. (3), (4) and (5)

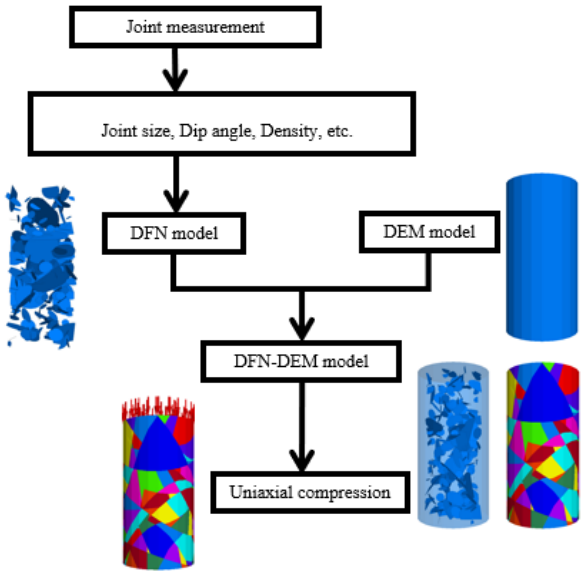

Fig. 2 Numerical simulation flow

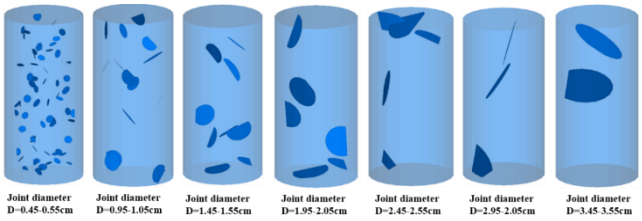

Fig. 3 DFN-DEM models of different joints distributions

$$P_{32} = P_{30} \times A \tag{3}$$

$$A = \pi \times \left(\frac{D}{2}\right)^2 \tag{4}$$

$$P_{32} = P_{30} \times \pi \left(\frac{D}{2}\right)^2 \tag{5}$$

where P_{32} is the joint density per unit volume, P_{30} is the number of joints per unit volume, A is the area of a single joint, V is the joint distribution region, S is the total area of the joints, and D is diameter of a single joint.

According to the above equation, when the joint density P_{32} per unit volume is constant, the number of joints P_{30} per unit volume is negatively correlated with the joint diameter D. Additionally, when the joint distribution area and joint density remain unchanged, the total area of the joints does not change. When the joint size increases, the number of joints decreases. Since the positions and the angles of the joints are random, the joints may not be uniformly distributed within the model; with more clustering of the joints, and the degree of dispersion decreases, as shown in Fig. 3.

By changing the diameter of the joint and then changing the distribution of the joint space, the statistical results of the uniaxial compressive strength of the rock mass are shown in Fig. 4.

The analysis shows that the difference between the

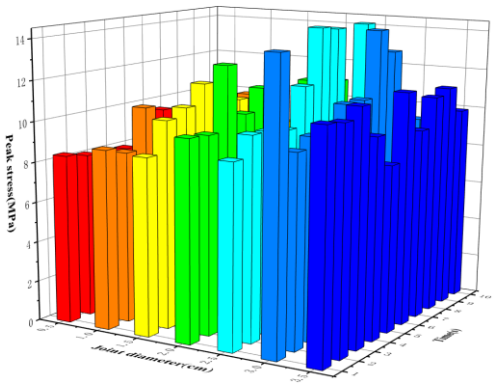

Fig. 4 The compressive strengths of rock masses with different spatial distributions of joints

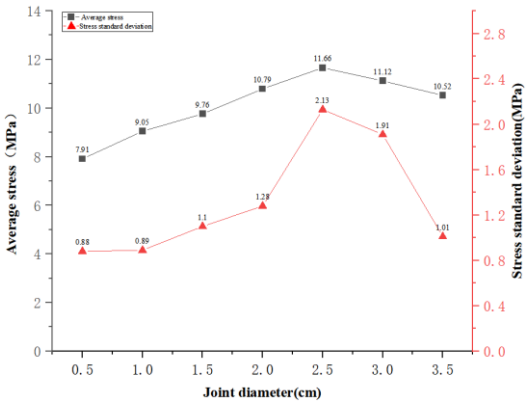

Fig. 5 The average value and standard deviation of the spatial distributions of the rock masses with different spatial distributions of the joints

maximum and minimum compressive strengths of the tested rock mass specimens with different joint diameters and spatial distributions is 2.98 MPa, 3.28 MPa, 3.54 MPa, 4.87 MPa, 5.37 MPa, 5.35 MPa and 3.30 MPa. These results, combined with the average value and standard deviation of the peaks in the spatial distributions of rock masses with different joints in Fig. 5, first monotonically increases and then monotonically decreases. Further analysis shows that when the joint diameter is 0.45-0.55 cm, the joints are small and numerous, and the spatial distribution range is wide, which weakens the overall structure of the rock mass and makes the rock mass compressive strength the lowest, at 7.92 MPa. In addition, with a large number of joints and limited space, the distribution of joints has little influence on the strength of rock masses. Therefore, the compressive strengths of jointed rock masses with different spatial distributions of the joints have little difference, with a standard deviation of 0.89. When the joint diameter is 2.45-2.55 cm, as the joint size increases, the spatial distribution tends to be clustered, and the rock mass is structurally weakened. When the compressive strength of the rock mass is 11.67 MPa, it is not easily damaged. As the number of joints decreases and the size increases, the nonuniformity of the spatial distribution increases. Under different spatial distribution forms, the fluctuation in the compressive strength of the rock mass also changes, and the standard deviation is 2.13. When the diameter of the joints is 3.45-

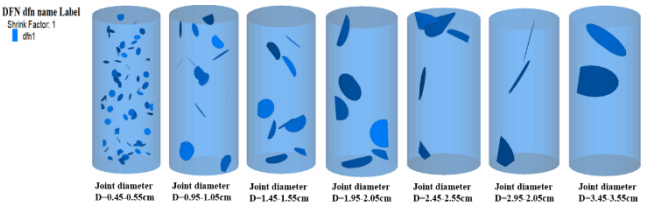

Fig. 6 Spatial distribution of different joints in a rock mass

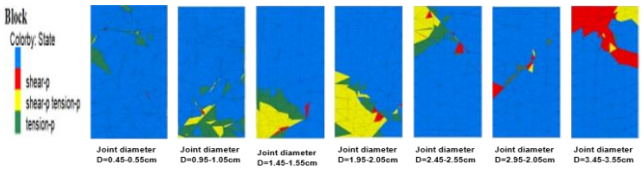

Fig. 7 Plastic zones of rock masses with different joint distributions

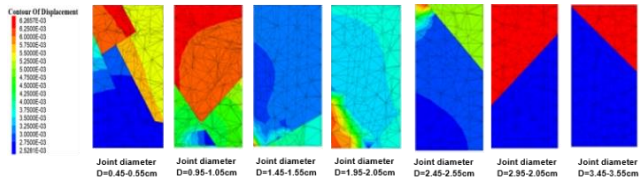

Fig. 8 Macroscopic displacement in rock masses with different joint

3.55 cm, the joints are large but few, the spatial distribution tends to be clustered, and the compressive strength of the rock mass gradually decreases to 10.53 MPa. At this diameter, the influence of joint size is the most obvious, and the rock mass is easily damaged. The influence of the spatial distribution form of the joints is reduced, but the influence of the spatial distribution form of the joints on the rock mass is not significant, and the standard deviation is only 1.01.

Based on the above analysis, the following conclusions can be drawn: When the joint density remains the same, “small but many” joints and “large but clustered” joints have the greatest impact on the strength of the rock mass. The former reduces the strength of the rock mass mainly by changing the structure of the rock mass, while the latter causes the failure of the rock mass mainly by further developing the joints.

3.2 Influence of the spatial distribution of joints on the failure mode of a rock mass

Fig. 6 shows the distribution of joints in rock masses with different joint densities. The blue circles in the figure represent the joints existing in the rock masses; Fig. 7 and Fig. 8 show the internal plastic zone profiles of the rock masses with different joint densities after failure under uniaxial compression and the macroscopic displacement diagrams of the rock masses respectively. As shown in Fig. 7 and Fig. 8, the density and location of the joints greatly affect the location and degree of the large deformation of the rock mass and the type and size of the plastic zone after rock mass failure.According to the observation of rock mass failure, there are three types of failure zones: The first type of failure zone fails along the joint surface; the second type is internal failure of the whole rock; the third type is failure along the joint surface and internal failure of the whole rock simultaneously. According to statistical analysis, the first and third types are more common, and the second type rarely occurs. The plastic zones of the rock masses in Fig. 7 can be divided into three types: shear plastic zones (red), tensile plastic zones (green) and tensile-shear mixed plastic zones (yellow). According to the type and size of the plastic zone after rock mass failure, the failure mode of the jointed rock mass is determined, and the influence of the joint density on the rock mass is analyzed. Fig. 6 shows the joint distributions of rock masses with different joint diameters from 0.45-0.55 cm to 3.45-3.55 cm, and the distribution of the joints gradually changes from dispersion to concentration with increasing joint diameter. Under uniaxial compression, the plastic zone and macroscopic displacement of the jointed rock mass change regularly with the change in joint distribution. The plastic zone after the failure of different jointed rock masses is shown in Fig. 7. When the stress of the jointed rock mass reaches its tensile or compressive limit, the rock mass begins to enter a plastic state, forming the plastic zone. Regardless of the size of the joint, a plastic zone forms inside the jointed rock mass after failure. The distribution of plastic zone varies with the size and distribution of the joints, among which the locations of the joints and the plastic zone at the edge of the rock mass are the most obvious. As shown in Fig. 6(a) and (b), when the joint diameters are 0.45-0.55 cm and 0.95-1.05 cm, the joints greatly decrease the structural integrity of the rock mass, and it is easier to destroy the rock mass during loading. To destroy the rock mass during loading. At the same time, due to the random joint distribution, the internal stress of the jointed rock mass is not uniform during the loading process. Considering the abovementioned diameter ranges, the corresponding plastic zones after failure are shown in Fig. 7 (a) and (b), respectively. The pure tensile plastic zone accounts for 80.03% and 65.12%, while the shear and tensile-shear plastic zones account for 19.03% and 12.45% and 0.94% and 22.43%, respectively. Therefore, the failure at this time is mainly tensile failure, and the overall failure form is shear slip failure along the joint plane. As shown in Fig. 8 (a) and (b), the small and scattered joints result in nonuniform, multidirectional and scattered deformation in the rock mass. When the joint diameters are 1.45-1.55 cm and 1.95-2.05 cm, the number of joints decreases, and the degree of dispersion decreases with increasing joint size. The corresponding joint distributions are shown in Fig. 6(c) and (d), respectively. The number of joints is moderate, and the joints are interlaced with each other so that the local structure of the rock mass is greatly damaged. Therefore, the distribution of the plastic zone is relatively concentrated, and the proportions of the tensile and shear plastic zones gradually increase to 51.39% and 75.96% of the plastic zone, respectively, as shown in Fig. 7(c) and (d). Therefore, the damage at this time is caused by tensile and shear. According to Fig. 8(c) and (d), due to local aggregation of the plastic zone, the deformation of the rock mass after failure is characterized by local crushing and large

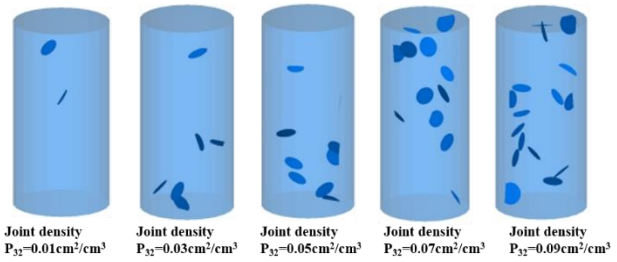

Fig. 9 DFN-DEM models with different joint densities

displacement. When the joint diameters are 2.45-2.55 cm, 2.95-3.05 cm, and 3.45-3.55 cm, as shown in Fig. 6(e), (f), and (g), with the increase in the joint size, the joints become large. At this time, the failure of the jointed rock mass is often caused by the further development of a single large joint during the uniaxial loading process. A shear failure surface is formed in the rock mass. On this failure surface, most of the rock masses produce shear displacement. Therefore, as shown in Fig. 7 (e), (f), and (g), the proportion of the pure shear plastic zone gradually increases to 7.48%, 45.36% and 81.26% of the plastic zone, respectively, and the position of the plastic zone is around the shear failure zone. According to Fig. 8(e), (f), and (g), the shear failure zone divides the rock mass into two parts. The macroscopic displacement of the rock mass produces large deformation and slip along the top of the joint plane, while the deformation under the joint plane is relatively small, and the rock mass maintains a good bearing capacity.

According to the above analysis, the joint size and joint density have a great influence on the failure mode and displacement deformation characteristics of rock masses: When the joints are small and well distributed, the rock mass failure is mainly tensile failure, and the displacement and deformation show multiangle and multidirectional characteristics. When the joints are large and sparse, the rock mass failure gradually changes from tensile shear to pure shear failure, and the displacement deformation becomes slip failure along the shear failure surface.

4. The influence of joint density on the mechanical properties of rock mass

4.1 The influence of joint density on the compressive strength of a rock mass

To study the influence of joint density on the compressive strength of the tested rock masses, the joint density is set to 0.01, 0.03, 0.05, 0.07, and 0.09 cm^2/cm^3, the joint diameter is set to a 1.0-1.1 cm power law distribution, and the joint position and angle are set to uniform distributions. As shown in Fig. 9, five different random models are generated under the condition of the same fracture network parameters with different densities.

When the joint density is 0.01 cm^2/cm^3, the standard deviation is 0.74. In this case, the number of joints in a unit area is small, and the distribution of joints is scattered. The peak stress is not easily affected by the distribution of the joints, and the difference between the maximum and

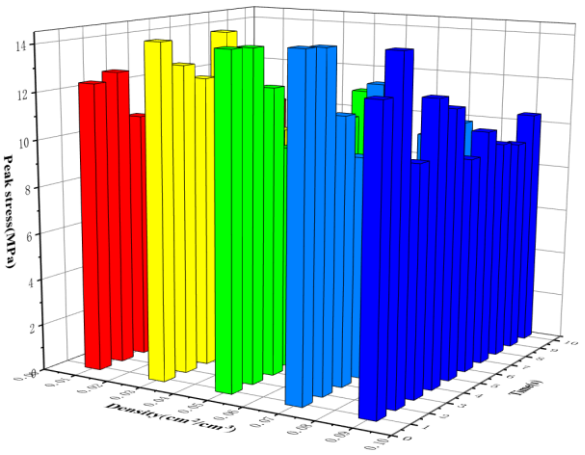

Fig. 10 Compressive strengths of rock masses with different joint densities

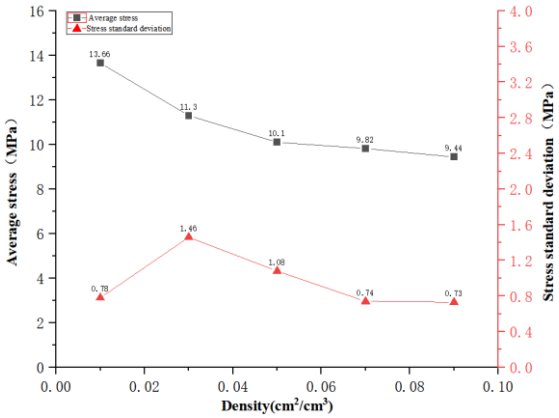

Fig. 11 Peak mean strength values and standard deviations of rock masses with different joint densities

minimum peak stresses is 2.03 MPa; when the joint density is 0.03 cm^2/cm^3, the standard deviation is 1.50. The number of joints in the rock mass is held constant, and the distribution of joints is varied to test many forms. The peak strength of the rock mass varies greatly among the simulations with the same characteristic parameters; the peak strength of the rock mass is most susceptible to the spatial distribution of the joints, and the difference between the maximum and minimum values is 4.81 MPa. With increasing joint density, the number of joints per unit area increases, and the peak stress of the jointed rock mass decreases. Under the influence of the joint distribution, the uniaxial compressive strength of the jointed rock mass tends to be stable, the standard deviation is 0.73, and the difference between the maximum and minimum values is 2.25 MPa. The compressive strength of the rock mass is affected by the spatial distribution of the joints with different joint densities. According to the broken line chart of the average peak strength of the jointed rock mass in Fig. 11, with increasing joint density, the strength and deformation parameters of the rock mass with different joint densities show a monotonically decreasing trend. As the joint density increases from 0.01 cm^2/cm^3 to 0.09 cm^2/cm^3, the peak strength of the rock mass decreases from 13.64 MPa to9.45 MPa, and then the peak strain decreases from

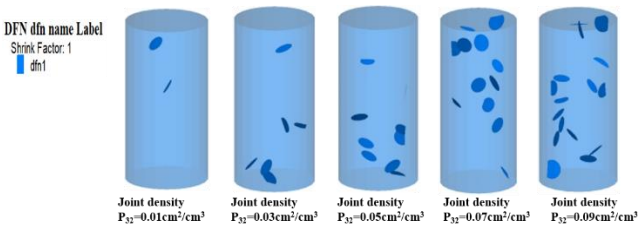

Fig. 12 Joint location distributions in rock masses with different joint densities

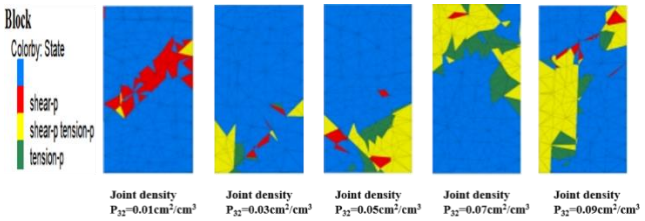

Fig. 13 Variation in the plastic zone properties of rock masses with different joint

2.61×10^{-3} to 1.66×10^{-3}. At the same time, the fragmentation degree of the rock mass increases, and the peak strength of the rock mass decreases by 17.23%, 10.66%, 2.7% and 3.9% when the joint density increases by increments of 0.02 cm^2/cm^3. This finding shows that when the joint properties of the rock mass reaches a certain threshold, the influence of joints on the strength of the rock mass gradually decreases.

4.2 The influence of joint density on the failure mode of a rock mass

In essence, the deformation and failure of a rock mass is caused by the propagation and coalescence of internal joints in the rock mass, and the existence of joints greatly affects the formation and development of the plastic zone in the process of rock mass failure. At the same time, due to the randomness and uncertainty in the joint distribution, the type, distribution and shape of the plastic zone are often irregular, which directly determines the failure form and degree of the rock mass. Determining the distribution and type of plastic zone inside a rock mass has important guiding significance for the deformation analysis of rock masses.

The joint distribution for the joint density of 0.01 cm^2/cm^3 is shown in Fig, 12(a), and with fewer joints, the joint spacing is larger. During the loading process, the possibility of rock bridges breaking between joints is low, which is usually manifested as single joint development. As is shown in Fig. 13(a), the shear plastic zone accounts for 91.33% of the plastic zone, and the tensile-shear plastic zone in the inclusion part accounts for 8.67%, forming a strip-shaped shear failure zone in the rock mass. Fig. 12(a) shows that the positions of the shear zone and the joints are consistent. According to Fig. 14(a), due to the appearance of a shear failure zone inside the rock mass, the macroscopic displacement of the rock mass presents shear slip along the joint plane. At this time, the rock mass below the joint plane retains a good structure and strong bearing capacity. When

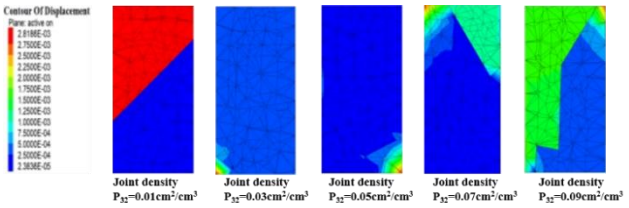

Fig. 14 Macroscopic displacements of rock masses with different model node arrangements

the joint density is 0.03 cm^2/cm^3 and 0.05 cm^2/cm^3, as shown in Fig. 12(b) and 12(c), local agglomeration occurs due to the increase in the number of joints, and the joint spacing decreases. The local influence on the rock mass is great, resulting in the phenomenon of local fragmentation. As shown in Fig. 13(b), the shear plastic zone, tensile shear plastic zone and tensile plastic zone are 11.15%, 69.96% and 18.89% of the plastic zone, respectively. As shown in Fig. 13(c), the shear plastic zone, tensile shear plastic zone and tensile plastic zone are 18.53%, 65.92% and 15.55% of the plastic zone, respectively. The main characteristics are tensile shear failure and local crushing, and the rock mass gradually produces local deformation under the vertical load. At the same time, due to the random distribution of joints, the joint orientation is not uniform, so the forces in rock mass are not uniform, and the dilatancy of joints is restricted to different degrees. The proportion of the tensile shear plastic zone increases gradually, which leads to different deformation degrees and model failure modes of the rock mass. Therefore, as shown in Fig. 14(b) and 14(c), the macroscopic displacement of the rock mass is mainly caused by the large local deformation in the joint clustering area, and the degree of deformation gradually decreases from the edge of the rock mass to the center.

When the joint density is 0.07 cm^2/cm^3 and 0.09 cm^2/cm^3, as the joint distribution area in Fig. 12(d) and 12(e) expands, the density gradually increases. As shown in Fig. 13(d), the tensile-shear plastic zone, tensile plastic zone and shear plastic zone are 13.5%, 57.49%, and 41.16% of the plastic zone, respectively, and as shown in Fig. 13(e), the tensile-shear plastic zone, tensile plastic zone and shear plastic zone are 5.91%, 77.28%, and 16.81% of the plastic zone, respectively. After loading failure, the tensile-shear plastic zone in the center of the joint is large and intersects the pure tension-plastic zone at the edge. Meanwhile, considering the macroscopic displacement of the rock mass in Fig. 14(d) and 14(e), due to the increase in the plastic zone area and shear failure zone area, the displacement and deformation of this rock mass are more severe than those of the low-density jointed rock mass, and the failure mode of the jointed rock mass is slip along the shear failure zone and local crushing. In short, with an increase in joint density, the jointed rock mass will produce greater displacement and deformation after compressive failure. If the plastic zone is connected to the shear failure zone and tensile failure zone, the probability of failure will be greatly increased. These parts are generally required in engineering applications. It can be seen from the above analysis that with the increase in joint density from 0.01 cm^2/cm^3 to 0.09 cm^2/cm^3, the proportions of three kinds of plastic zones and the

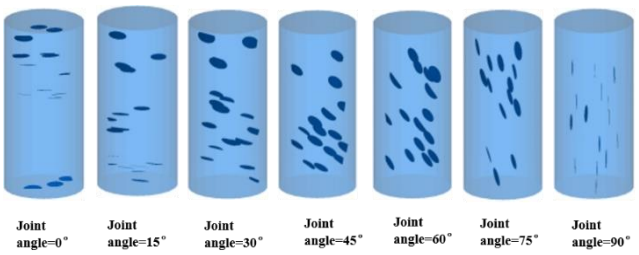

Fig. 15 Rock pillar models of composite rock masses with different joint angles

macroscopic displacements of rock masses with different joint densities show regular changes after compressive failure. As shown in Fig. 13 and Fig. 14, when the joint density is small, the plastic zone of the rock mass is mainly a pure shear plastic zone and forms a shear failure zone. The macroscopic displacement of the rock mass is manifested as sliding failure along the shear failure zone. With increasing joint density, the plastic zone changes from a pure shear plastic zone to a tensile-shear plastic zone. Therefore, the failure mode of the rock mass also changes from shear slip along the fracture zone to a mixed mode of local large deformation and global slip. At the same time, considering the location distribution and density of the joints in the rock mass in Fig. 12, the existence of joints greatly weakens the structure of the rock mass and affects the mechanical properties and bearing capacity of the rock mass.

5. The influence of joint angle on the mechanical properties of a rock mass

5.1 The influence of joint dip on the compressive strength of a rock mass

To study the influence of joint dip angle on rock pillar strength, the joint dip angle is incrementally increased from 0° to 90°, to simulate fifteen angles, while the other parameters remain unchanged. When the joint density is set to 0.09 cm^2/cm^3, the joint diameter is determined by a power distribution of 1.0-1.1 cm, and the position of the joints is determined by a random distribution. As shown in Fig. 15, under different angles and the same fracture network parameters, seven different random models are generated.

The joint dip angle is incrementally increased from 0° to 90°, to simulate fifteen angles, while the other parameters remain unchanged. When the joint density is set to 0.09 cm^2/cm^3, the joint diameter is determined by a power distribution of 1.0-1.1 cm, and the position of the joints is determined by a random distribution. As shown in Figure 15, under different angles and the same fracture network parameters, seven different random models are generated.

The statistical results of the peak stresses of the tests can be obtained through data sorting of the results of each test, as shown in Fig. 16. Through calculation, the joint inclination angle is increased from 0° to 90°, and the differences between the maximum and minimum peak

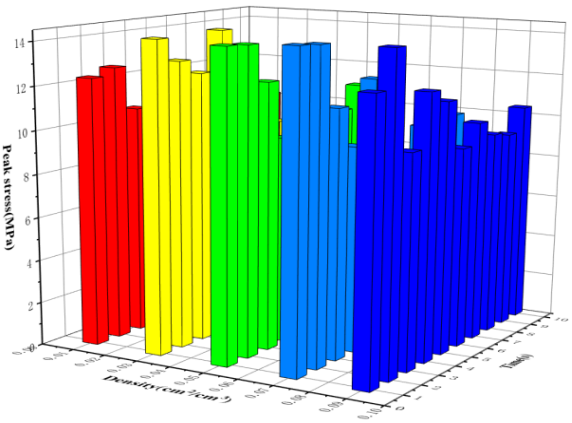

Fig. 16 Compressive strengths of rock masses with different joint angles

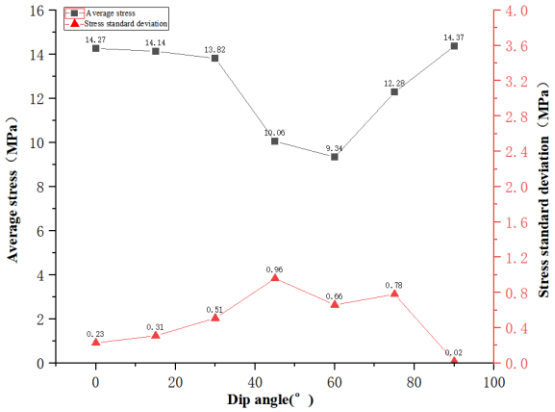

Fig. 17 Peak mean and standard deviation results of the strengths of rock masses with different joint angles

stresses of the rock masses are 0.74 MPa and 0.78 MPa, 1.70 MPa, 3.34 MPa, 2.11 MPa, 2.86 MPa, 0.08 MPa. The mean value and standard deviation curves of the peak stress can be obtained by statistical analysis of the test results of each group of specimens with the same angle. As shown in Fig. 17, the dispersion of the peak stresses obtained in the tests changes during the simulation process. When the joint angle increases from 0° to 45°, the dispersion degree of the peak stresses of the rock masses at different angles increases gradually; the standard deviation increases from 0.23 to 0.96. Then, the dispersion degree decreases gradually. When the joint angle is 90°, the dispersion degree of stress is the lowest, at 0.02, and the overall M-shaped trend changes. When the joint inclination angle is small or large, the bearing capacity of the fractured rock mass is less affected by its internal joint distribution, and the compressive strengths of different joint distributions are basically the same. When the joint inclination angle is between 45° and 75°, the distribution characteristics of the joint have a great influence on its bearing capacity. When the angle is known, the spatial distribution form of the joint should be paid more attention.

Fig. 17 shows that the strength of the jointed rock masses with different dip angles varies with the dip angle. When the joint angle increases from 0° to 30°, the numerical simulation of the strength of the jointed rock

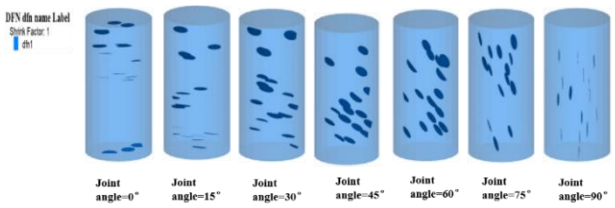

Fig. 18 Joint location distribution in rock masses with different joint

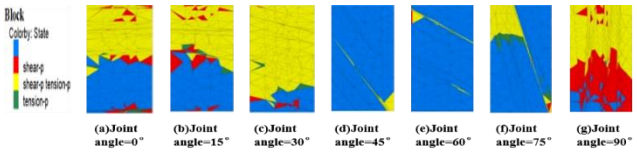

Fig. 19 Variation diagram of plastic zone of rock mass with different joint

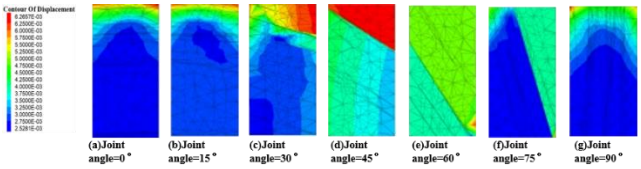

Fig. 20 Macroscopic displacements of rock masses with different joint properties

mass changes slightly, from 14.27 MPa to 13.83 MPa, which is only 0.44 MPa. When the joint angle increases from 30° to 60°, the strength of the jointed rock mass begins to decrease rapidly and reaches the minimum value of 9.34 MPa, and the reduction range is 4.43 MPa. When the joint angle is increased to 90°, the strength of the joint rock mass begins to gradually increase to the maximum value of 14.37 MPa. The jointed rock mass strength results show a "U"-shaped change rule; combined with the theoretical strength curve of a single structural plane, when the joint angle increases from 0° to α_1=25.9°, there is little difference between the strength of the rock mass and that of the joint, and the influence of the joint angle is small. When the angle increases from 30° to $\pi/5+\psi/2$=57.95°, the theoretical strength decreases sharply to the minimum value. The theoretical strength begins to increase as the angle increases to α_2=75°. When the joint angle continues to increase from α_2=75° to 90°, the strength of the jointed rock mass is consistent with the strength of the intact rock again and generally shows a "U" pattern. It can be seen from the numerical simulation peak strength curve and theoretical strength curve that the variation rules of the two curves are very consistent. When the joint angle increases from 0° to 90°, the two curves show the same change rule.

Joints with dip angles of 0~15° have little effect on the strength of the simulated rock masses. When the dip angle is between 45° and 60°, the change in the angle has a greater impact on the strength of the rock mass; however, when the angle is 60~90°, the strength of the rock mass changes greatly. When the angle is between 30° and 75°, the strength of the rock mass is relatively low. In Fig. 17, the strength "sag area" is formed, and the strength drops to the lowest point at 60°.

The above analysis suggests that the numerical simulation curve is basically consistent with the theoretical strength curve of a single structural plane, and the numerical valued are close, too. Therefore, it can be considered that the model in this paper can better simulate the change in strength a jointed rock mass.

5.2 The influence of the joint angle on the failure mode of a rock mass

According to the analysis in Section 5.1, the strength of jointed rock masses shows a U-shaped change pattern with increasing joint angle, and the strength theory of a single structural plane has certain applicability in the determination of the strength of rock masses with multiple joints. Therefore, on the basis of the above analysis, this section further analyzes the influence of the joint angle on the failure mode of rock masses by combining the observations of the plastic zone formed after rock mass failure and the displacement variation diagram.

The joint distributions for joint angles of 0°, 15° and 30° are shown in Fig. 18(a), (b) and (c). Considering the plastic zone results in Fig. 19(a), (b) and (c), it can be seen that the main part of the plastic zone is the tensile-shear plastic zone, which accounts for 85.72%, 81.35% and 95.82%, respectively, in addition to the 11.85%, 15.53%, and 2.37% shear plastic zone and 2.43%, 4.12%, and 1.81% tensile plastic zone. Thus, if the joint angle is less than 30°, then the joint rock mass mainly undergoes tensile-shear failure, and only a small amount of pure shear and pure tensile failure occurs. Moreover, with the continuous increase in the joint angle, the area of the tensile shear plastic zone increases gradually, the bearing capacity of the rock mass decreases gradually, and the proportion of tensile shear failure increases. Meanwhile, according to the macroscopic displacements of the rock masses in Fig. 20(a), (b) and (c), when the joint dip angle is less than 30°, the deformation of the rock mass mainly weakens from top to bottom, and the vertical displacement trajectories are arched. Farther from the center of the rock mass, the deformation is smaller, and there is an obvious end effect. When the joint angle is 30°, the displacement of the rock mass will gradually increase along the joint plane. When the joint angles are 45°, 60° and 75°, as shown in Fig. 18(d), (e) and (f), the main feature of the plastic zone is that a shear failure zone appears in the rock mass, and the shear failure zone and joint dip angles are consistent.

When the joint angle is 75°, there is a local plastic concentration zone at the end of the shear failure zone near the edge of the rock mass. According to the macroscopic displacements shown in Fig. 20(d), (e) and (f), due to the increase in the joint angle, the macroscopic displacement of the rock mass mainly occurs via slip deformation along the shear failure zone. At this time, the rock mass is divided into two parts, and there is a certain anti-slip force and bonding force between the joints, leading to the transmission of discontinuous displacement. The joint distribution for a joint angle of 90° is shown in Figure 18(g). The joints and loading are parallel, cutting the rock mass into multiple column-like bodies. The distribution

characteristics of the plastic zone are again dominated by tensile shear, accounting for 89.87% of the plastic zone, and the shear plastic zone accounts for 10.13%. The area of the plastic zone reaches the maximum value under these conditions, and the rock mass failure is mainly caused by tensile-shear failure. With reference to Fig. 20(g), the displacement and deformation of the rock mass again show that the displacement is gradually weakened from top to bottom and that the vertical displacement is distributed in an arch shape. Farther from the center of the rock mass, the deformation is smaller.

According to the above analysis, under the condition of uniaxial compression, the failure conditions of different angles in the jointed rock mass model mainly show that when the dip angles of the joints are less than the friction angle and equal to 75°, the plastic zone area increases gradually from top to bottom and the macroscopic displacement of the rock mass is tensile failure from the end of the rock mass downward with local crushing. When the joint angle is between 45° and 75°, a shear failure zone forms in the plastic zone, and the macroscopic deformation of the rock mass is mainly a mixed mode of sliding along the shear failure plane with local crushing (Yong *et al*. 2018).

6. Conclusions

In this paper, the influence of the joint parameters on the mechanical properties and failure modes of jointed rock masses in nonpersistent fracture networks is studied.Based on the SRM technology and three-dimensional discrete elements, 3DEC three-dimensional discrete element software is used to construct a discrete fracture network (DFN) and a block discrete element model (DEM), and the corresponding joint parameters can controlled. Based on the DFN-DEM model, simulation experiments are carried out to study the influence of joint size, joint density, joint occurrence and other parameters on the equivalent mechanical parameters of fractured rock masses. The preliminary research conclusions are as follows:

(1) We obtain the influence of the mechanical parameters of the jointed rock mass on the strength and failure mode of the jointed rock mass through simulation tests. This shows that synthetic rock mass technology based on three-dimensional discrete elements can be used to study the effect of joint density, joint occurrence, joint dispersion degree, joint size, and joint dip angle. The corresponding mechanical property and failure analyses are feasible (Yang *et al*. 2021).

(2) As the size of the joints in a rock mass increases, the compressive strength and dispersion of the rock mass first increase and then decrease. Among them, the joint characteristics of “small but many” joints and “large but clustered” joints have the most significant impact on the strength of the rock mass. The resulting rock mass strengths with joints of different sizes are different. With the increase in the joint density in a rock mass, the compressive strength of the rock mass decreases monotonically, but the rate of decrease slows gradually. With the increase in the joint angle in the rock mass, the strength parameter of the rock mass first decreases and then increases, forming a U-shaped change rule, and the degree of dispersion first increases and then decreases.

(3) In analyzing the failure mode and deformation analysis of a jointed rock mass, the type of plastic zone after failure is closely related to the macroscopic displacement and deformation of the rock mass and the distribution of the joint parameters. When the joint angle is less than or equal to 90°, below the friction angle, the plastic zone of the rock mass mainly undergoes tensile-shear failure, and the displacement decreases gradually from top to bottom. When the joint angle is greater than the friction angle and less than 90°, a shear zone is formed in the rock mass, and the deformation of the rock mass is sliding along the shear zone. The shear zone divides the rock mass into two parts. The lower the joint density, the easier it is to produce shear failure. In addition, a shear failure zone is formed along the joint area, along which the rock mass slips and deforms. The greater the density of joints, the more likely it is that tensile-shear failure will occur. Failure surfaces or shear failure zones are formed in rock masses with dense joints, and the rock mass is deformed into local crushing and slippage along the shear failure zones. “Small but many” joints are more prone to rock bridge fracture and tensile failure. The rock mass deformation is scattered and controlled by the joint and plastic zone distributions. When the joints are “large and clustered,” further development of the joints produces a shear zone, which causes the rock mass to slip and fail along the shear zone.

Acknowledgments

The research of this study was sponsored by the State Key Laboratory of Mining Response and Disaster Prevention and Control in Deep Coal Mines (SKLMRDPC20KF02), the National Natural Science Foundation of China (52074166) and the China Postdoctoral Science Foundation (2019M652436). The authors are grateful for their support.

References

Bo, H.U. (2010), “Intelligent selection of mechanical of discontinuous jointed rock mass based on Ffine structure descriptions and numerical tests”, Chinese Journal of Rock Mechanics and Engineering, Doctoral Dissertation, Ph. D. Thesis, Institute of Geology and Geophysics, Chinese Academy of Sciences, Beijing.

Cheng-Fu, G.U. and Wang, H. (2015), “numerical simulation of rock failure process under different crack distribution under action of compressive stress”, Coal Technology.

Cho, J.W., Kim, H., Jeon, S. and Min, K.B. (2012), “Deformation and strength anisotropy of Asan gneiss, Boryeong shale, and Yeoncheon schist”, *Int. J. Rock Mech. Min. Sci.*, **50**, 158-169. https://doi.org/10.1016/j.ijrmms.2011.12.004.

Deng, G., Xie, H., Gao, M., Li, C. and He, Z. (2020), “Numerical simulation on the evolution of mining-induced fracture network in a coal seam and its overburden under the top coal caving method”, *Adv. Civil Eng.*, **2020**, Article ID 8833193.

https://doi.org/10.1155/2020/8833193.

Esmaieli, K., Hadjigeorgiou, J. and Grenon, M. (2010), "Estimating geometrical and mechanical REV based on synthetic rock mass models at Brunswick Mine", *Int. J. Rock Mech. Min. Sci.*, **47**(6), 915-926. https://doi.org/10.1016/j.ijrmms.2010.05.010.

Fu, J.W., Zhang, X.Z., Zhu, W.S., Chen, K. and Guan, J.F. (2017), "Simulating progressive failure in brittle jointed rock masses using a modified elastic-brittle model and the application", *Eng. Fract. Mech.*, **178**, 212-230. https://doi.org/10.1016/j.engfracmech.2017.04.037.

Harthong, B., Scholtès, L. and Donzé, F.V. (2012), "Strength characterization of rock masses, using a coupled DEM-DFN model", *Geophys. J. Int.*, **191**(2), 467-480. https://doi.org/10.1111/j.1365-246X.2012.05642.x.

Huang, J., Safari, R., Lakshminarayanan, S., Mutlu, U. and McClure, M. (2014), "Impact of discrete fracture network (DFN) reactivation on productive stimulated rock volume: Microseismic, geomechanics and reservoir coupling", *48th US Rock Mechanics/Geomechanics Symposium. OnePetro*, June.

Huang, Y.H. (2016), "An experimental study on fracture mechanical behavior of rock-like materials containing two unparallel fissures under uniaxial compression", *Acta Mechanica Sinica*, **32**(3), 442-455. https://doi.org/10.1007/s10409-015-0489-3.

Huang, Y.H. and Yang, S.Q. (2015), "Discrete element study on strength and failure behavior of jointed sandstone with two sets of cross-joints", *J. China Coal Soc.*, **40**(1), 76-84.

Inc, I. (2013), 3DEC-3D Distinct Element Code, Version 5.0, User's Manual.

Ivars, D.M., Pierce, M.E., Darcel, C., Reyes-Montes, J., Potyondy, D.O., Young, R.P. and Cundall, P.A. (2011), "The synthetic rock mass approach for jointed rock mass modelling", *Int. J. Rock Mech. Min. Sci.*, **48**(2), 219-244. https://doi.org/10.1016/j.ijrmms.2010.11.014.

Li, S., Wang, G., Wang, S., Yang, W. and Wang, X. (2006), "Application of fracture-damage model to anchorage of discontinuous jointed rockmass of excavation and supporting", *Chin. J. Rock Mech. Eng.*, **25**(8), 1582-1590.

Li, Y., Zhou, H., Dong, Z., Zhu, W., Li, S. and Wang, S. (2018), "Numerical investigations on stability evaluation of a jointed rock slope during excavation using an optimized DDARF method", *Geomech. Eng.*, **14**(3), 271-281. https://doi.org/10.12989/gae.2018.14.3.271.

Liu, S.G., Liu, H.N., Wang, S.J., Hu, B. and Zhang, X.P. (2008), "Direct shesar tests and PFC2D numerical simulation of intermittent joints", *Chin. J. Rock Mech. Eng.*, **27**(9), 1828-1836.

Mughieda, O.S. (1997), "Failure mechanisms and strength of non-persistent rock joints", University of Illinois at Urbana-Champaign.

Olofsson, I. and Fredriksson, A. (2005), "Strategy for a numerical Rock Mechanics Site Descriptive Model. Further development of the theoretical/numerical approach", Technical Report, SKB-R-05-43, Sweden.

Qing-Bin, M.E.N.G., Li-Jun, H.A.N., Wei-Guo, Q.I.A.O., Deng-Ge, L.I.N. and Lie-Chang, W.E.I. (2012), "Numerical simulation of cross-section shape optimization design of deep soft rock roadway under high stress", *J. Min. Saf. Eng.*, **29**(5), 650-656.

Shu, J., Jiang, L., Kong, P. and Wang, Q. (2019), "Numerical analysis of the mechanical behaviors of various jointed rocks under uniaxial tension loading", *Appl. Sci.*, **9**(9), 1824. https://doi.org/10.3390/app9091824.

Wang, J. *et al.* (2019), "Analysis of damage evolution characteristics of jointed rock mass with different joint dip angles", Journal of Harbin Institute of Technology.

Wang, P.X., Cao, P., Pu, C.Z., Fan, X. and Wang, C.C. (2017), "Effect of the density and inclination of joints on the strength and deformation properties of rock-like specimens under uniaxial compression", *Chin. J. Eng.*, **39**(4), 494-501.

Yang, H., Liu, B. and Karekal, S. (2021), "Experimental investigation on infrared radiation features of fracturing process in jointed rock under concentrated load", *Int. J. Rock Mech. Min. Sci.*, **139**, 104619. https://doi.org/10.1016/j.ijrmms.2021.104619.

Yin, S.H., Wu, A.X. and Li, X.W. (2012), "Orthogonal polar difference analysis for sensitivity of the factors influencing the ore pillar stability", *J. China Coal Soc.*, **37**, 48-52.

Zeng, L. *et al*. (2019), "Optimization of loosing circle support of stoping roadway with large inclination", *Mod. Tunnel. Technol.*, **56**(3), 102-107.

Zhao, Y., Wu, Y., Xu, Q., Jiang, L., Huang, W., Zhang, P. and Niu, Z. (2020), "Numerical analysis of the mechanical behavior and failure mode of jointed rock under uniaxial tensile loading", *Adv. Civil Eng.*, **2020**, Article ID 8811282. https://doi.org/10.1155/2020/8811282.

Zhu, W.C., Tang, C.A., Yang, T.H. and Liang, Z.Z. (2003), "Constitutive relationship OF mesoscopic elements used in RFPA~(2D) and its validations", *Chin. J. Rock Mech. Eng.*, **22**(1), 24-29.

CC